


# In-situ monitoring of powder bed fusion of polymers using laser profilometry

**Journal Article****Author(s):**

Sillani, Francesco ; MacDonald, Eric; Villela, Janely; Schmid, Manfred; Wegener, Konrad

**Publication date:**

2022-11

**Permanent link:**

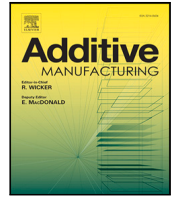
<https://doi.org/10.3929/ethz-b-000568662>

**Rights / license:**

[Creative Commons Attribution 4.0 International](#)

**Originally published in:**

Additive Manufacturing 59, <https://doi.org/10.1016/j.addma.2022.103074>



## Research paper

## In-situ monitoring of powder bed fusion of polymers using laser profilometry

Francesco Sillani<sup>a,b,\*</sup>, Eric MacDonald<sup>c,d</sup>, Janely Villela<sup>c</sup>, Manfred Schmid<sup>a</sup>, Konrad Wegener<sup>b</sup><sup>a</sup> Inspire, Innovation Center for Additive Manufacturing Switzerland (icams), 9014 St.Gallen, Fürstentlandstrasse 122, Switzerland<sup>b</sup> Swiss Federal Institute of Technology, ETH Zürich, Institute of Machine Tools and Manufacturing (IWF), 8092 Zürich, Leonhardstrasse 21, Switzerland<sup>c</sup> The University of Texas at El Paso, El Paso, TX, USA<sup>d</sup> Manufacturing Science Division, Oak Ridge National Laboratory, Oak Ridge, TN, USA

## ARTICLE INFO

## Keywords:

Polymer powder bed fusion  
 Process monitoring  
 Curling  
 Powder bed density  
 Powder bed roughness

## ABSTRACT

Process monitoring allows for unique opportunities to capture information at intermediate layers during fabrication for part qualification, but also to improve process robustness by identifying issues before yield or quality is reduced. An industrial-grade laser profilometer has been integrated for the first time in a commercial polymer laser sintering machine and used to monitor powder bed quality and potentially qualify parts during production. Powder layer quality was measured in different conditions and changed drastically as a function of recoating speed, preheating temperature but also particle shape. The effective layer thickness was obtained for the first time in PBF of polymers, and gradually increased with the layer count until reaching a plateau at the nominal layer thickness. Powder layer density could be calculated as well and lies between 34 and 65 %, depending on the powder type and layer count. Finally, curling increased with decreasing preheating temperature, ranging from 70  $\mu\text{m}$  to 350  $\mu\text{m}$  i.e. until collision with the recoater. Based on the measured degree of curling, mitigation strategies could be integrated using a closed-loop feedback control. Effective process monitoring such as the one provided with laser profilometry may enable the development of new materials featuring more complex processing conditions, but also larger machines where thermal uniformity might be an issue.

## 1. Introduction

The production of plastic components with additive manufacturing for industrial applications is already a reality in selected fields. In particular, parts produced with powder bed fusion (PBF-LB/P), commonly known as laser sintering (LS), meet industrial requirements but further adoption of LS in industrial process chains is still hindered by a lack of in-process quality assurance measures. Specifically, there are currently hardly any suitable solutions for in-line process monitoring during ongoing build jobs, aside for monitoring and closed-loop control of surface temperature and laser parameters, and sometimes normal cameras which can only identify dramatic failures, such as cracks on the powder bed which could be also identified with a naked eye [1]. It is clear that process monitoring is key for successfully bringing additive manufacturing towards industrial standards. As AM is a primary forming technology, design is created together with material properties, and thus defects induced by the production process are directly transferred in the final parts. On the other hand, working layer-by-layer offers a unique opportunity to control the quality of components by closely monitoring process performances during production with the ultimate goal of achieving process certification.

In this work, the application of laser profilometry during processing of polymer powders in an industrial machine is explored: here, an industrial monitoring device is used to provide effective feedback thanks to high-resolution 3D data that can be used in quasi-real-time for powder bed quality and parts quality assurance.

Productivity is a key aspect for every manufacturing technology, and being AM a layer-by-layer process, productivity can be enhanced by reducing the number of layers e.g. by using an higher nominal layer thickness, or by reducing the duration of a single layer. This is greatly influenced by part bed size, recoating speed and of course part complexity (through the scan strategy). Data shown in Fig. 1 report the average time spent at each stage every layer (Recoat, Heat, Expose) for an EOS P110 [2] (200 mm along the recoating direction) and an EOS P500 (500 mm) [3] with a similarly packed build job (about 10%), and were obtained as motivation for the current work.

The exposure time varies with the complexity of the layer/part, while heating and recoating times are (mostly) independent of the build job and can be assumed as more related to powder properties and machine setup. The heating time is mainly influenced by the thermal

\* Corresponding author at: Swiss Federal Institute of Technology, ETH Zürich, Institute of Machine Tools and Manufacturing (IWF), 8092 Zürich, Leonhardstrasse 21, Switzerland.

E-mail address: [sillanif@ethz.ch](mailto:sillanif@ethz.ch) (F. Sillani).

<https://doi.org/10.1016/j.addma.2022.103074>

Received 3 April 2022; Received in revised form 18 July 2022; Accepted 4 August 2022

Available online 18 August 2022

2214-8604/© 2022 The Author(s). Published by Elsevier B.V. This is an open access article under the CC BY license (<http://creativecommons.org/licenses/by/4.0/>).

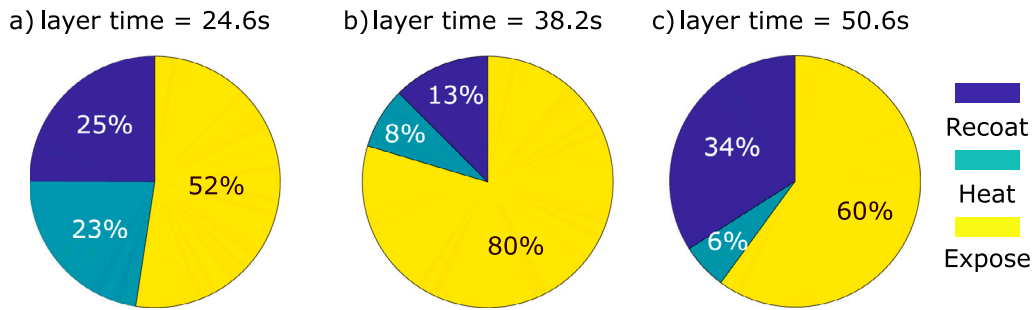


Fig. 1. Breakdown of average layer time for (a) EOS P110 at 125 mm s<sup>-1</sup> (b) EOS P500 at 450 mm s<sup>-1</sup> and (c) EOS P500 at 125 mm s<sup>-1</sup>.

conductivity of the polymer powder, while the recoating time could be lowered by adjusting the recoating speed or the recoater itself in order to maintain constant layer quality. Massive efforts were made by producers to minimize the recoating and heating time, and this is particularly evident when comparing Fig. 1a with (b): thanks to the quick recoating speed and powder pre-heating, the laser stays on for more than 80% of the layer time. Comparison between (a) and (c) shows a 136% increase in the relative importance of the recoating time with constant recoating speed 125 mm s<sup>-1</sup> and 250% build platform size, and it is clear that only perfectly-optimized powders can be spread at the top speed of the EOS P500, which of course comes at a price. In fact, [4] ran discrete element modeling (DEM) simulations on polymer powders, reporting a decrease of packing density with increasing recoating speed. [5] reported that illumination parameters (laser power, speed etc.) should be optimized for powder packing density, which has to be constant in the different layers that constitute the part. The powder packing state was studied also for composite material powders [6], where (at least) two different classes of particles are present: matrix and reinforcement, which in the case of fibers is characterized by a very different aspect ratio compared to the matrix. [6] reported also a detrimental effect of high recoating speed on packing density from DEM simulations, which is also influenced by layer thickness and content of fibers. [7] reported a detrimental effect of recoating speed on packing density, and even on final part quality and mechanical properties, showing e.g. a sharp increase (+33%) of Charpy impact strength upon higher (+10%) packing density. Therefore, a higher recoating speed is desirable for productivity, but has a detrimental effect on the packing density, which is a predictor for the final part density [8]. [9] experimentally measured a decrease of powder layer density ( $\rho_p$ ) with increasing recoating speed for several materials that are commercially available for PBF-LB/P.

The effective layer thickness  $ELT$  and its consistency throughout the build job is another key metric for quality assurance: particular combinations of laser parameters and powder properties (e.g. powder layer density) could lead to unacceptable variations of  $ELT$ , which might lead to inhomogeneous part properties. Also, not so many authors studied the melt pool depth evolution during selective laser sintering, and no one did that during actual processing using an industrial machine and a relatively inexpensive process monitoring tool. For example, [10] studied the melt pool depth during single line scans as a function of laser power using optical coherence tomography, with a complex setup on a research-grade machine, and reported values from 20  $\mu$ m to 200  $\mu$ m for  $ELT$ . Nevertheless, in this work the availability of high-resolution data before and after laser scanning concerning the vertical shrinkage of the powder layer into a molten state (along  $Z$ ) allows for the first time the determination of  $ELT$  for a complex geometry, introducing the possibility of measuring an interesting metric for process stability [11].

Curling is a form of thermally-induced warpage that is recognized as one of the most problematic types of defects occurring in PBF-LB/P, in which a stress is induced with the introduction of cold powder and results in the part lifting from the powder bed [7]. [12] reported a



Fig. 2. Curling illustration. The material which is not affected by the laser is depicted in black.

convincing explanation for curling, together with a theoretical model derived from laser bending of sheets. The temperature gradient mechanism (TGM) introduced by these authors is based on the rapid heating of the top layer of powder by the laser, which tries to expand but is constrained by the lower layer of colder material, resulting in layer-wise bending as shown in Fig. 2. Curling is affected by several factors, including part geometry, orientation, positioning in the build chamber and process parameters [13], but also material properties, such as the low thermal conductivity of polymer powders, which changes with packing density [14]. Curling can occur during the build phase (built-in curl) or upon cooldown (post-build curl) [13]. [15] recently integrated a camera in a commercial PBF-LB/P machine and used machine learning methods to identify and quantify powder bed defects such as agglomeration but the dataset used did not allow conclusive findings. Machine-learning based image analysis was also studied by [1] on a commercial Sintratec machine, but applicability of camera-based techniques is always questionable since no height data were natively available. Curling has been studied in-process for PBF of polymers also by [16], who mounted a fringe projection monitoring system outside of a EOS P100 machine, successfully measuring parts with a  $XYZ$  resolution of 75  $\mu$ m on a large portion of the build chamber, demonstrating that the naked eye of the operator is sometimes insufficient to identify curling. More interestingly, by tuning process parameters, namely part bed temperature and laser energy density, the researchers demonstrated the control of curling and even repairing parts on-the-go, reducing the probability of a catastrophic failure i.e. a recoater collision with the part. Unfortunately, no information were provided on the data acquisition time and/or surface map analysis, raising questions regarding the applicability as a real-time process monitoring tool. In this work, the focus is only on built-in curl, since laser profilometry can be used to detect geometrical variations with sub-micrometer vertical resolution. A common strategy to mitigate built-in curl is to increase the preheating temperature of the powders in the feeders, but excessive heat can result in increased powder cohesiveness, leading to the formation of clumps. Consequently, mitigation strategies for defects like curling certainly exist but are mainly related to the experience of the operator, since an automatic optimization of the production process is not yet possible, mainly due to a lack of reliable height data and time-efficient data processing. The availability of comprehensive height mapping through innovative process monitoring tools will enable the

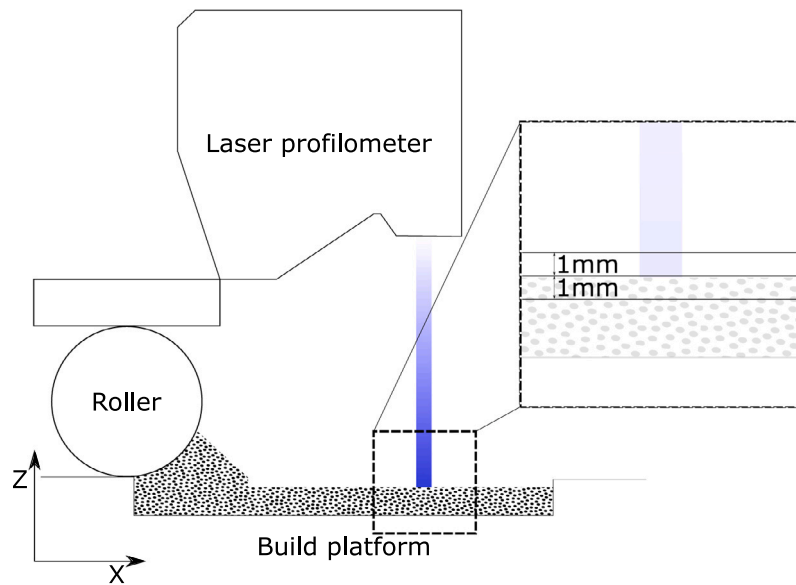


Fig. 3. Sketch of the mounting principle of the laser profilometer on the recoater arm of the Sinterstation 2000, with details of the field of view in the dashed square.

**Table 1**  
Key information about Keyence LJ-X8060.

Laser wavelength	405 nm
Spot size	25 mm × 49 μm
Linearity	0.008%
Profile data interval	10 μm
Line length	16 mm
Acquisition frequency	1 kHz to 16 kHz

development of new materials with more complex processing conditions i.e. narrower sintering windows, but also for the development of larger machines where thermal uniformity would become increasingly more challenging with size.

The scope of this work is to provide an overview of the different possible applications of laser profilometry in powder bed fusion of polymers, by focusing on powder layer quality, a predictor for powder bed density, on curling, a common defect occurring in PBF-LB/P, and for the first time also on in-situ measured effective layer thickness (ELT) and powder layer density ( $\rho_p$ ). Although laser profilometry has been explored for process monitoring of powder bed fusion of metals [17], this work focuses on polymer powder bed fusion, which is more challenging due to the high build chamber temperatures.

## 2. Materials and methods

### 2.1. Measuring setup

A Keyence LJ-X8060 (Osaka, Japan) laser profilometer was integrated into a DTM Sinterstation 2000. To allow precise information extraction from the powder bed, which is characterized by a lack of reference points, encoding was necessary and realized with a temperature-resistant linear encoder along the recoating direction ( $X$ ) coupled with proper tuning of the laser profilometer settings (along  $Y$ ). Due to this setup, an  $XY$  resolution of 10 μm was obtained, while the vertical one (along  $Z$ ) is 0.45 μm according to the device datasheet, over a vertical ( $Z$ ) field of view of 2 mm in the configuration shown in Fig. 3.

Additional parameters of the laser profilometer are reported in Table 1.

Since the PBF-LB/P process occurs with a build chamber temperature between 80 °C and 170 °C (material-dependent), a cooling enclosure with nitrogen flow was implemented to protect the laser

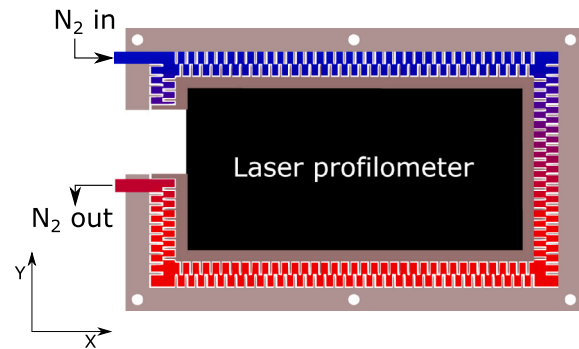


Fig. 4. Sketch of rig specifically designed for the laser profilometer which allows high temperature operation thanks to nitrogen cooling.

**Table 2**  
 $PSD$  (in μm), Young's modulus  $E$  (in MPa) and Ultimate Tensile Strength  $\sigma_{UTS}$  (in MPa)

Material	$D_{10}$	$D_{50}$	$D_{90}$	$E$	$\sigma_{UTS}$
DF-PA12	28	56	82	1586	43
iCoPP	35	63	123	900	18

profilometer, as depicted in Fig. 4. A bidirectional connection between the control unit of the laser profilometer and the machine Programmable Logic Controller (PLC) was realized, allowing for the dynamic adjustment of certain process parameters and automatically trigger the acquisition of the surface maps based on the position of the recoating arm.

### 2.2. Powder bed quality evaluation

Three variables were selected for the study on powder bed quality: recoating speed, build chamber temperature and materials. Two grades were chosen: Duraform PA12 (3D Systems, Rock Hill, SC, USA), a polyamide 12 which is the most used feedstock in PBF-LB/P [18] with a melting point around 175 °C, and iCoPP, a polypropylene co-polymer featuring a melting point of about 125 °C. Additional information are reported in the following Table 2, with the Particle Size Distribution  $PSD$  hereby given with the 10th, 50th and 90th diameter percentiles.

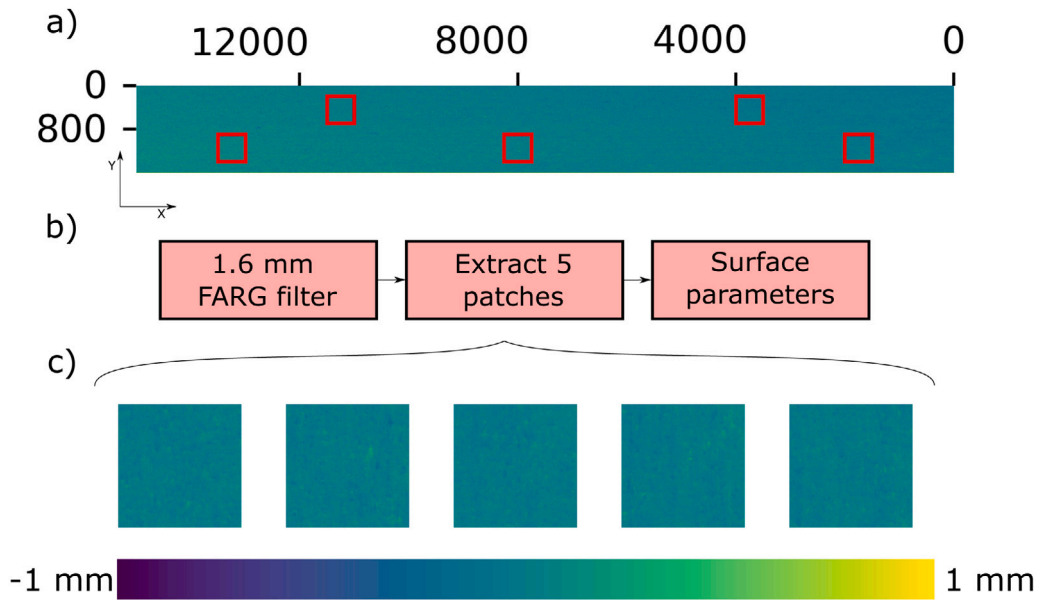


Fig. 5. Raw data (a) is filtered with a Gaussian filter and five patches are extracted (b–c). The height parameter  $S_q$  is then calculated for each patch, which measures  $5 \times 5$  mm.

Both materials are commercially available and feature a wide sintering window [19]. The feedstock was used as received, without preconditioning and in virgin form (no mixing with used powder).

In terms of build chamber temperature, three different build temperatures (processing, processing  $-20^\circ\text{C}$ , processing  $-40^\circ\text{C}$ ) and three different recoating speeds ( $80, 120$  and  $160\text{ mm s}^{-1}$ ) were covered, for a total of nine pairs of experimental conditions, each of them tested over the recoating of ten layers. Every dataset was analyzed using an in-house developed Python script to extrapolate the powder bed roughness, evaluated using  $S_q$  calculated according to Eq. (1), as schematically shown in Fig. 5.

$$S_q = \sqrt{\frac{1}{A} \iint_A z^2(x, y) dx dy} \quad (1)$$

where  $z$  is the height distribution,  $x$  and  $y$  the coordinates of each data point and  $A$  the area of the region in mm.

All the statistical evaluation were executed using Matlab. For ANOVA, the normality assumption was checked with Shapiro–Wilk and the homoscedasticity with Levene tests, in both cases with rejection of the null hypothesis when  $p < 0.05$ . In case either of the two tests were not significant, bootstrapping was performed to reduce bias, with a number of bootstrapped data samples equals to the sample size of each group. When comparing different groups, the means were compared according to Tukey–Kramer and their difference considered significant when  $p < 0.05$ .

### 2.3. Part evaluation during processing: effective layer thickness, powder layer density and curling

The same laser profilometer was also used to characterize parts during production using the following metrics:  $ELT$ ,  $\rho_p$  and degree of curling ( $\theta$ ). In the curling experiments, data acquisition occurred after the new layer of powder was deposited (Fig. 6b), while for obvious reasons the  $ELT$  had to be measured before recoating (Fig. 6a). With the current setup it is not possible to measure both curling and  $ELT$  at the same time, but this can be solved by mounting an additional laser profilometer on both sides of the recoater arm, or by measuring  $\theta$  and  $ELT$  alternatively.

#### 2.3.1. Effective layer thickness evaluation

For  $ELT$ , a different setup of the laser profilometer was used: in this case, the actual polymer melt pool was scanned. A specific test geometry was made, consisting of 13 cylinders with diameter 10 mm aligned along  $X$  and spanning over the entire build platform, as shown in Fig. 6a. After scanning of the layer, the test part was measured and the height difference  $h_n$  was obtained as median distance between the two planes shown in Fig. 7:

Once  $h_n$  is known,  $ELT$  can be obtained geometrically according to Eq. (2):

$$ELT_{L_n} = h + h_{n-1} - h_n \quad (2)$$

where  $h_{n-1}$  is the height difference measured in the previous layer,  $h$  is the platform movement that is also equal to the height of the new layer of powder, and  $h_n$  is the height difference measured in the current layer. This equation is explained in Fig. 8:

In the first step (a), a fresh layer of powder with height  $h$  is present. After laser scanning, the first height difference  $h_0$  is measured with the laser profilometer (b). Then, the platform is lowered by  $h$  and a new layer of powder (always of height  $h$ ) is deposited (light blue in c). The machine laser selectively melts the cross section of the part, and hence the next layer  $L_1$  is obtained. Therefore, the next height difference  $h_1$  can be measured with the laser profilometer (d). In this example,  $ELT_{L_1}$  is obtained by  $h_0 + h - h_1$ , and the process can be repeated for the next layer  $L_2$  (e and f), and so on.

From the theoretical point of view, the evolution of effective layer thickness  $ELT$  was never analyzed in PBF-LB/P, but other authors did that in PBF of metals [11,20,21].

A comparison of the layer-by-layer evolution of  $ELT$  and  $\delta_{p|n}$  (according to [20]) can be seen in Fig. 9, obtained for different values of powder layer density  $\rho_{p|n}$  and constant  $h = \delta_{l|n+1} = 100 \mu\text{m}$ :

Therefore, constant  $ELT$  should be reached within 6 to 24 layers in PBF-LB/M, depending on  $\rho_{p|n}$ . Nevertheless, in PBF of polymers, no build plate is used and the first layer is directly obtained from powder: this means that the main assumption of [20] regarding the first layer height is not respected, since there is no constraint that prevents the powder from melting in an uncontrolled way in the vertical direction. [22] reported a decreasing penetration depth of the  $\text{CO}_2$  laser radiation in polyamide 12 powder of  $220 \mu\text{m}$  to  $90 \mu\text{m}$  with increasing powder bed density from 30% to 65%. Therefore, a plausible first layer thickness lies between these extreme values, however, due to



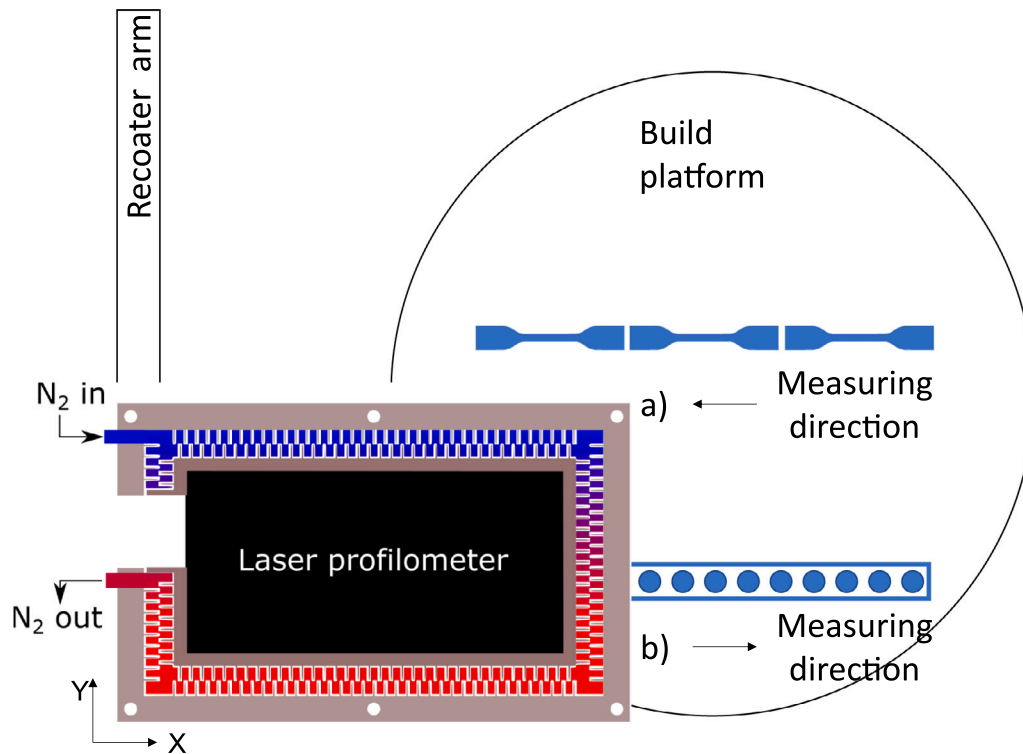


Fig. 6. Positioning and data acquisition direction of (a) the test geometries for curling (ISO 527-5 A specimens) (b) the *ELT* test geometry.

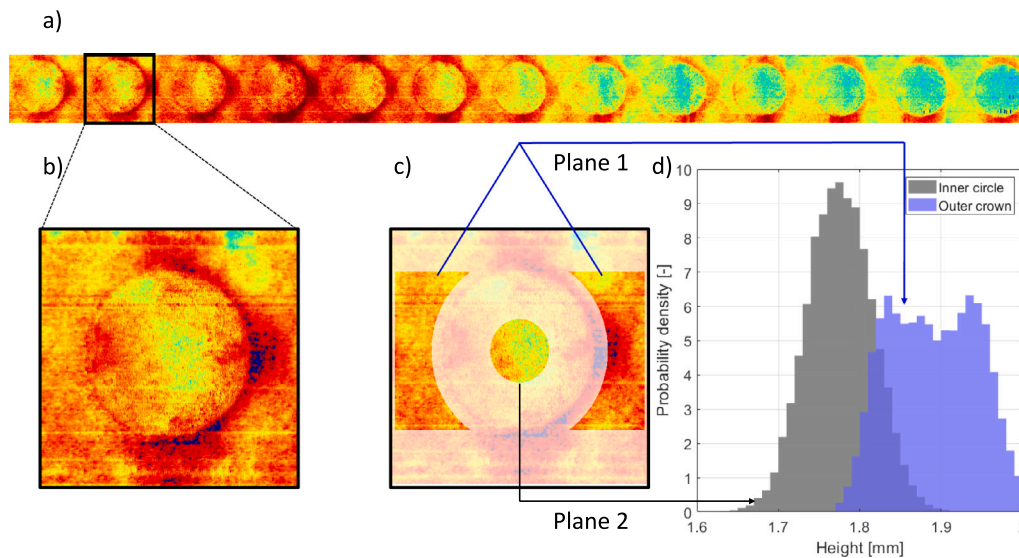


Fig. 7. Height measurement process for every part. Starting from the entire scan (a), each circle was isolated (b) and the planes for the height measurement selected (c). Plane 1 corresponds to the unmolten powder, plane 2 to the melt pool. The histogram (d) clearly shows the difference in the height distributions.

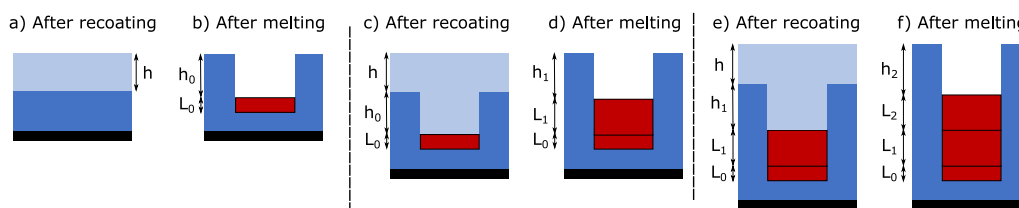


Fig. 8. ELT calculation from actual and previous height difference measurement. Build platform in black, fresh powder in light blue, existing powder in blue, molten layers in red. (For interpretation of the references to color in this figure legend, the reader is referred to the web version of this article.)

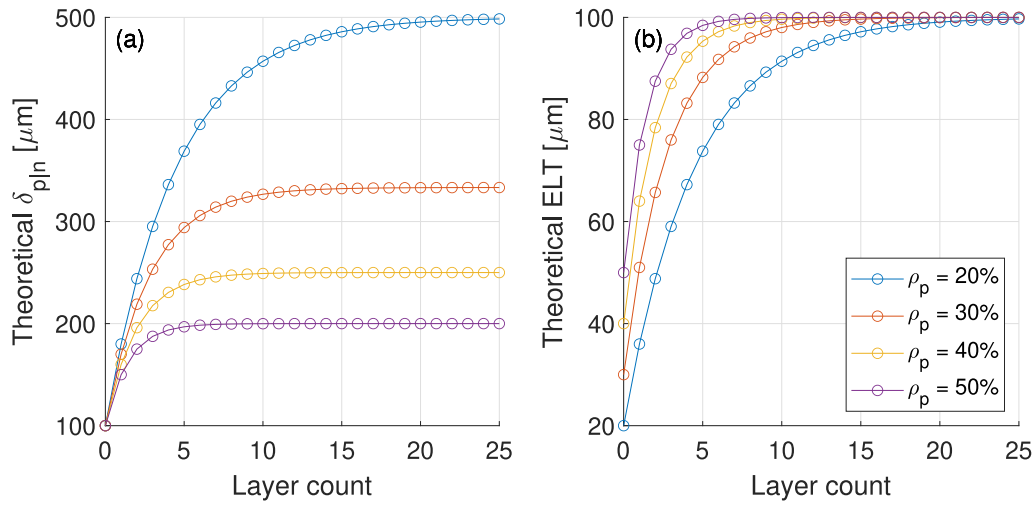


Fig. 9. Theoretical evolution of  $\delta_{p|n}$  (a) and  $ELT$  (b) with constant interlayer  $\rho_{p|n}$ .

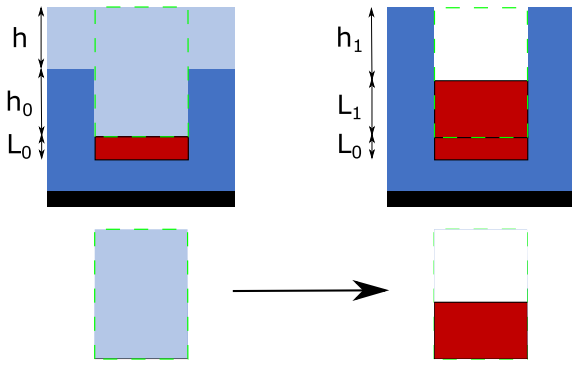


Fig. 10.  $\rho_p$  calculation from  $ELT$  data.

the peculiarity of the approach used to measure  $ELT$  in this work, it cannot be determined experimentally. Nevertheless, the second layer would be indeed constrained vertically by the first one, so a drop of  $ELT$  is expected before reaching a certain steady state around  $h$ .

### 2.3.2. Powder layer density evaluation

Since the cross section of the part in the  $XY$  plane can be assumed to be roughly the same before and after the melting process, and the conservation of mass applies between the volumes highlighted with a green, dashed outline in Fig. 10, the relation

$$(h + h_{n-1}) \cdot \rho_p = ELT_{L_n} \cdot \rho_{melt} + h_n \cdot 0 \quad (3)$$

must hold.

Therefore, the effective powder layer density  $\rho_p$  can be obtained in absolute units if the melt density  $\rho_m$  is known:

$$\rho_p = \rho_{p|n} = \frac{ELT_{L_n}}{h + h_{n-1}} \cdot \rho_{melt} \quad (4)$$

The melt density of polymers varies with temperature, since the polymer chains tend to expand when heated. Melt density data are not easy to identify for a specific polymer grade, and therefore an average value for each polymer type was used in this work:  $0.97 \text{ g cm}^{-3}$  for Duraform PA12 (polyamide 12) and  $0.74 \text{ g cm}^{-3}$  for iCoPP (copolypropylene) [23].

Of course, the  $ELT$  hereby measured is not precisely the one of the part, since crystallization and shrinking upon cooling can lead to differences, and vertical shrinkage of about 1% to 3% was reported for LS [24]. Therefore, the difference between the  $ELT$  calculated in

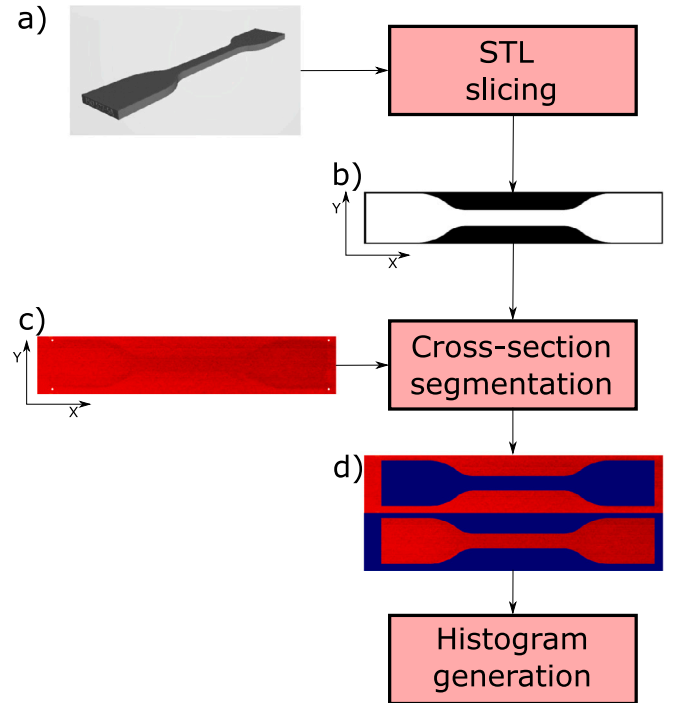


Fig. 11.  $\theta$  measurement process for every layer. The STL file is sliced (a), the correct cross-section is extracted for that specific layer (b) and used to segment (d) the raw data (c).

this work and the “real”  $ELT$  is negligible, under the assumption of constant interlayer shrinkage. So, this methodology allows to ascertain with good precision the absolute packing density of the powder during production, an important metric associated to part quality in powder bed fusion of polymers [8,9].

### 2.3.3. Curling evaluation

OpenCV libraries were leveraged in Python to analyze the raw data coming from the laser profilometer, as schematically depicted in Fig. 11.

A 2D bit mask template for each layer was generated by slicing the intended 3D geometry, provided as an STL file (a). In the case of the tensile bar, the template is the same for all layers, as shown in (b), where each pixel represents a square of  $100 \mu\text{m}^2$ . Template matching

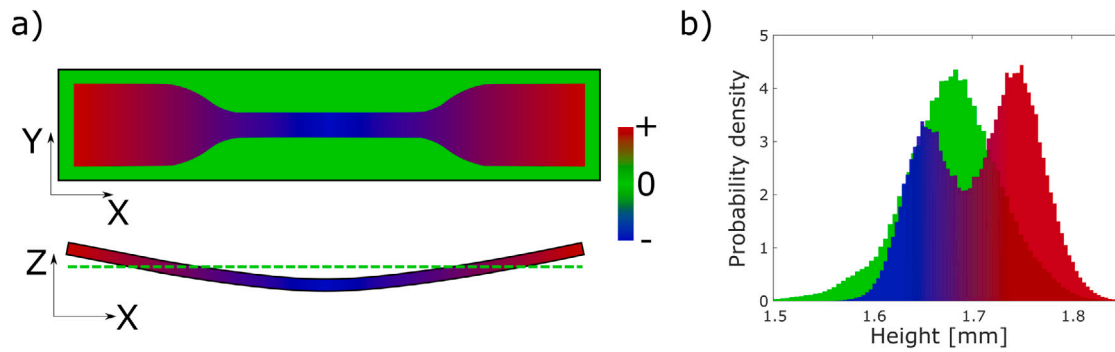


**Fig. 12.** Curling illustration in PBF of polymers. (a) shows an example of deformation with respect to the reference plane, while (b) quantifies those deformations in two distributions using the segmentation procedure introduced above. (For interpretation of the references to color in this figure legend, the reader is referred to the web version of this article.)

was employed to sweep the template across the layer depth data and identify the location providing the highest absolute correlation. When the PBF process runs without issues, the depth data should include a tight height distribution, as shown in (c), where the cross-section of the tensile bar is hardly recognizable. With the template location identified, pixels can be sorted as either inside or outside of the intended geometry as shown in (d).

Ideal data would look like the example reported in Fig. 12a, where curling occurs on a part and results in positive and negative vertical deflections (depicted in red and blue, respectively). The reference plane i.e. the unmelted powder is depicted in green. Thanks to the segmentation, it is possible to separate the overall height distribution in two, as shown in Fig. 12b.

Interestingly, a bi-modal height distribution would characterize all parts affected by curling, as hypothesized by [12]. These authors reported the creation of tensile stresses on top and compressive ones at the bottom of parts during cooldown in PBF-LB/M: in the case of polymers, though, the stresses come are the result of the deposition of cold powder on top of the molten part, and are immediately released due to the lack of a physical connection to the build plate, leading to part's deformation. In order to quantify it, the following Eq. (5) was used:

$$\theta = P_{95}(z_{part}) - \max(z_p) \quad (5)$$

where  $P_{95}(z_{part})$  is the 95-th percentile of the part height distribution (blue-red) and  $\max(z_p)$  is the peak of the powder height distribution (green). The whole data analysis takes about 30 s on a normal laptop, which is roughly within the layer time and thus offers relatively quick control possibilities.

### 3. Results and discussion

#### 3.1. Powder surface roughness

The surface roughness of Duraform PA12, spread at different temperatures (130 °C, 150 °C and 170 °C) and recoating speeds, is shown in Fig. 13a, while the grouped plots for speed and temperature are reported in Fig. 13b and Fig. 13c, respectively:

Qualitatively, Fig. 13a displays two clear trends: at the same temperature, increasing the recoating speed increases the surface roughness; however, across different temperatures, the average value of  $S_q$  at the different speeds is constant. In order to better quantify these behaviors, one-way ANOVA was carried out to determine the influence of speed and temperature separately, according to the methodology reported above. The contrast analysis shows that all combinations of temperatures and speeds are different from each other in a statistically significant way, as reported in Table 3, where positive differences in the means are linked to a smoothing effect of an increase of that variable.

**Table 3**  
Contrasts for Duraform PA12.

	Measurements group 1	Measurements group 2	Difference of means	p value
Speed [mm/s]	80	120	-0.41	0.00
	80	160	-1.34	0.00
	120	160	-0.93	0.00
Temperature [°C]	130	150	0.38	0.00
	130	170	0.53	0.00
	150	170	0.15	0.00

**Table 4**  
Contrasts for iCoPP.

	Measurements group 1	Measurements group 2	Difference of means	p value
Speed [mm/s]	80	120	-0.49	0.01
	80	160	-0.30	0.17
	120	160	0.18	0.49
Temperature [°C]	80	100	-4.51	0.00
	80	120	-3.77	0.00
	100	120	0.75	0.00

This statistical data highlights that changing either the recoating speed or the feeder temperature has an influence on the surface roughness, and the independent contribution of the two variables can be visualized in Fig. 13b and c, respectively. So increasing temperature to the processing region has a smoothing effect on the surface roughness  $S_q$  and thus the resulting powder layer density would increase [9]. On the other hand, increasing the recoating speed has a negative effect on the surface smoothness, and thus decreases  $\rho_p$ . Also the variance of  $S_q$  increases, which means that layer quality is less constant with increasing recoating speed, and thus recoating defects such as voids etc. are more probable.

Surface roughness of iCoPP has been tested under different conditions of temperature (80 °C, 100 °C and 120 °C) and recoating speed, as shown in Fig. 14a:

The same procedure carried out for Duraform PA12 was applied, and the outcome of the contrast analysis is shown in Table 4, while the means of speed and temperature are reported in Fig. 14b and 14c:

The data reported in Table 4 show a negative (and statistically significant) effect on  $S_q$  when increasing recoating speed from 80 mm s<sup>-1</sup> to 120 mm s<sup>-1</sup>. The other two contrasts are not significant, hence one could say that increasing the recoating speed does not influence  $S_q$  and therefore the powder layer density for iCoPP. This lack of influence is probably due to the particle shape of this material [25], which is highly spherical and thus is not effected by recoating speed, at least within the tested range. This was already reported by [4], who ran DEM simulations on polymer particles with different shapes at different recoating speed, using a blade as recoating medium. In their



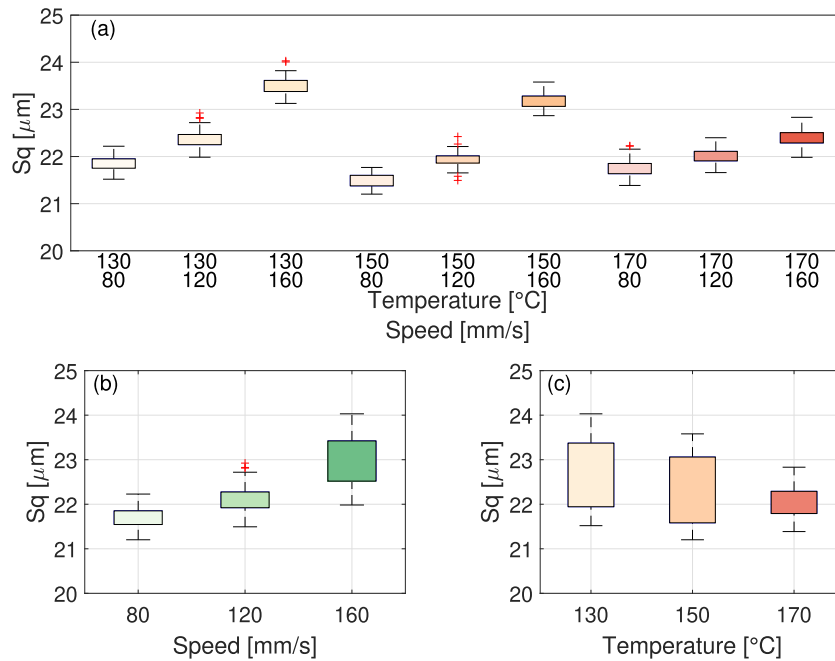


Fig. 13. Duraform PA12 — Surface roughness vs. temperature and speed (a), mean plots for speed (b) and temperature (c).

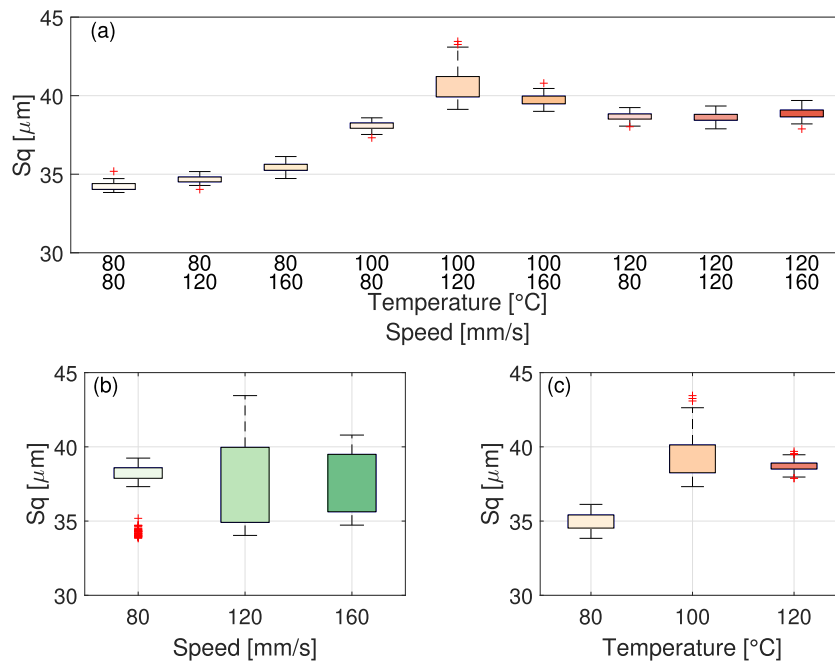


Fig. 14. iCoPP — Surface roughness vs. temperature and speed.

work, these authors showed an insignificant change of powder bed roughness with increasing recoating speed for spheres (iCoPP), while more irregular particles (like Duraform PA12) are more affected by a change of recoating speed. The results presented in Figs. 13 and 14 confirm those trends experimentally and in a statistically-significant way.

On the other hand, temperature does have a significant influence on surface roughness across all three values, as qualitatively depicted in Fig. 14(c). In fact, an increase of surface roughness could be observed between 80 °C and 100 °C, followed by a small (albeit statistically significant,  $p < 0.001$ ) decrease between 100 °C and 120 °C. This means that the corresponding packing density decreases with temperature, following the opposite trend of Duraform PA12.

This different behavior might be related to different relative magnitudes of the cohesive forces which keep the particles together, which means that powder cohesiveness changes with temperature [26], so flowability testing at room temperature gives only a rough indication of real powder behavior at the processing temperature. Furthermore, it seems that two commercially-available materials have significantly different behavior when recoating speed and temperature are changed, proving once more that a fundamental understanding of powder properties at the processing temperature is paramount to gain more knowledge about the powder bed fusion process itself.

For process monitoring purposes, the available range of recoating speeds provided by the used machine is not enough to obtain significant differences for iCoPP, although this might not be true for every other

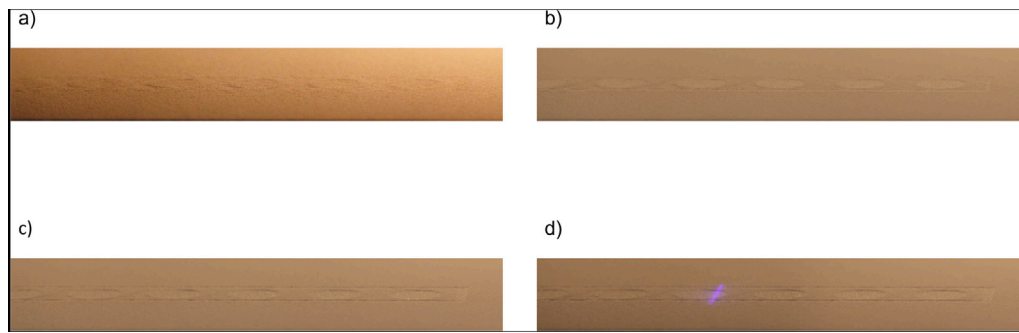


Fig. 15. Data acquisition sequence: powder bed just after recoating, with traces of the previous layer barely visible (a), illumination with CO<sub>2</sub> laser (b) and clear melting of the polymer powder (c), laser profilometer scanning (d).

**Table 5**  
Process parameters for *ELT* evaluation.

Parameter	Duraform PA12	iCoPP
Laser power [W]	35	30
Hatch [mm]	0.24	0.24
Laser speed [mm s <sup>-1</sup> ]	4000	4000
Layer thickness [μm]	100	100
Recoating speed [mm s <sup>-1</sup> ]	80	80
Part bed temperature [°C]	173	120
Feeder temperature [°C]	80	45

combination of temperature and recoating speed. Nevertheless, the methodology hereby proposed seems to be suitable for new feedstock development, whose flowability optimization at the processing temperature and recoating speed is crucial for successful materials in powder bed fusion of polymers.

### 3.2. In-situ effective layer thickness and powder bed density measurement

Using the methodology illustrated in Section 2.3, data were collected in a single build job, carried out under stable processing conditions according to the parameters reported in Table 5 with Duraform PA12 and iCoPP.

One data acquisition sequence example is depicted in Fig. 15.

Every layer constituting the test geometry was characterized independently, and therefore 13 melt pools were produced along  $X$ . Since the PBF-LB/P process does not use a substrate or build plate, it is impossible to calculate the thickness of the initial layer with the proposed methodology, because Eq. (2) requires a reference height measure. Moreover, due to the machine setup with powder feeders on both sides, only one every two layers could be measured. All individual melt pools are shown in Fig. 16:

Using the procedure introduced in Section 2.3, each melt pool was analyzed and used to calculate *ELT* and  $\rho_p$ . Fig. 17 reports the variation of *ELT* in the  $X$  direction as an average of all the layers (i.e.  $Z$  positions) for both Duraform PA12 (blue) and iCoPP (green). For neither of these two there exists a significant difference between left and right side of the platform (ANOVA  $p = 0.1$  for both).

The evolution of *ELT* along the  $Z$  direction is reported in Fig. 18:

For Duraform, the contrasts between  $n = 1$  and the other layers are all significant with  $p < 0.001$ , while there is no difference among the groups  $n > 2$ , except for  $n = 11$ . Regarding iCoPP, the contrasts between  $n = 1$  and all the other positions are also significant, with  $0.001 < p < 0.03$ , and again there is no difference among the groups  $n > 2$ , in this case with the exception of  $n = 17$ . This means that, for both materials, the first measured layer (which is the second layer of the part) is significantly different from the others, but its *ELT* does not follow the geometrical series proposed by [11] for PBF-LB/M. This was largely expected, since no build platform hinders the melting in the vertical direction, and thus the first *ELT* of the part is probably

even larger than the nominal thickness of the powder layer, due to uncontrolled penetration depth of the laser radiation. It is noteworthy though that a convergence towards the nominal layer thickness can be qualitatively seen in Fig. 18. For  $n = 17$  (iCoPP) and  $n = 11$  (Duraform PA12), a mechanical issue related to the piston movement has probably happened. In fact, Eq. (2) prescribes a fixed value for  $h$ : considering the age of PBF machine used in this work, the required precision cannot be guaranteed and would allow to explain these outliers.

Finally, an effect was observed around the contours of some of the melt pools with constant  $X$  and increasing  $Z$ , as can be qualitatively seen in Fig. 19 for Duraform PA12.

The powder surrounding the melt pool is raised for about 100 μm by the excess heat coming from the melting process, which makes it expand in the only unconstrained direction i.e. upwards. This can be considered as an indication that the energy density used is too high, and would enable closed-loop feedback not only for the recoating process but also for the laser/heater combination.

The determination of powder layer density (PLD) was carried out by using the procedure illustrated in Section 2.3. As explained above, the result can be expressed as a percentage of the melt density  $\rho_m$  or as an absolute value, if  $\rho_m$  is known. Fig. 20 reports the variation along  $X$  for both materials:

Similarly to *ELT*, no statistically significant difference can be observed in neither of the two materials along  $X$ . Nevertheless, for Duraform a negative trend ( $-5\%$  and  $-0.04 \text{ g cm}^{-3}$ ,  $p = 0.01$ ) can be found when comparing  $X \in (1 \dots 5)$  with  $X \in (8 \dots 13)$ , meaning that a  $\rho_p$  difference exists along the recoating direction for this material. This difference is probably related to the fact that the PSD of the powder changes in the recoating direction, with a progressive loss of its fine fraction particles. [5] already reported the need for a constant  $\rho_p$  across the platform, and this issue seems to be present also in this dataset: with larger machines, which are necessary to increase productivity, this behavior might get worse and therefore it is quite important to have a process monitoring tool capable of assessing the  $\rho_p$  in real time. At  $X = 9$ ,  $\rho_p$  drops significantly for iCoPP and insignificantly for Duraform: an hypothesis for such a behavior might be that the recoater moved vertically (bumped) in that specific location, shifting somehow the profilometer readings. Further tests are definitely required to exclude mechanical issues like this during build job execution.

The vertical evolution of  $\rho_p$  along  $Z$ , averaged for  $X$ , is shown in Fig. 21:

In both cases, a statistically significant difference arises between top and bottom layers: an increase of packing efficiency with layer count is quite counter intuitive, since *ELT* does not change between these two groups and therefore the powder has always almost the same empty volume to fill. Also, processing conditions are not changing between these two groups of layers. This different packing regime of the powder seems to be influenced by the homogeneous increase of temperature that occurs around the process region due to the extra energy provided by the laser, and whose effects were already observed

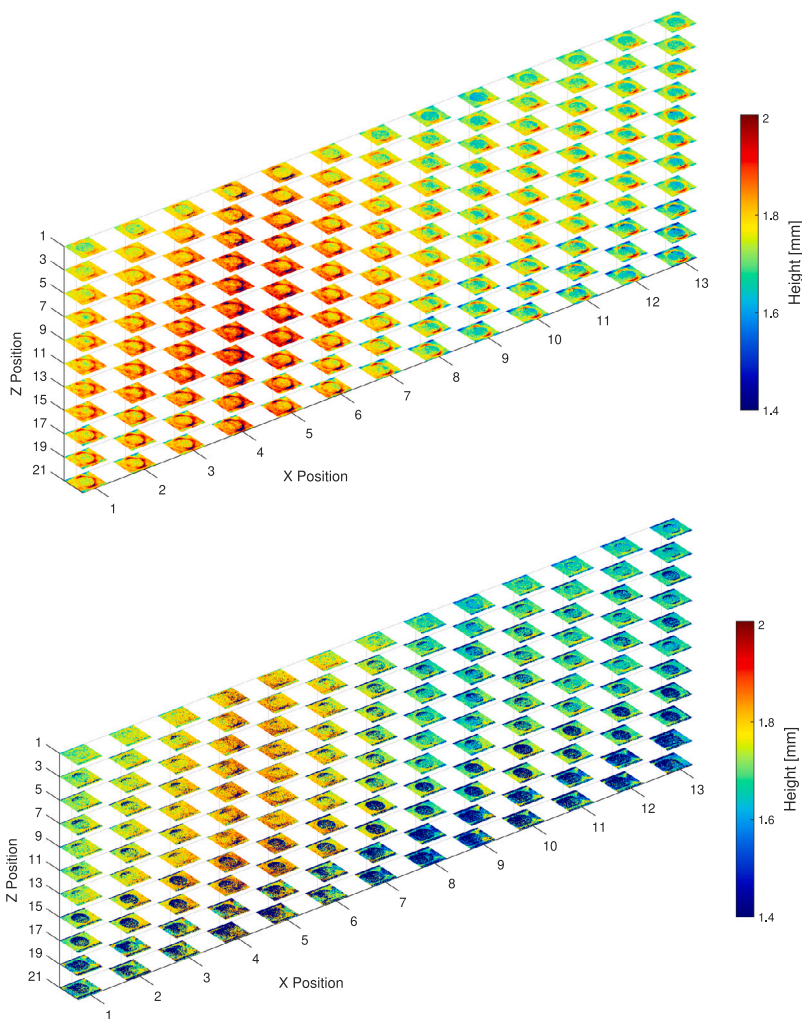


Fig. 16. Top — Duraform PA12 dataset; Bottom — iCoPP dataset.

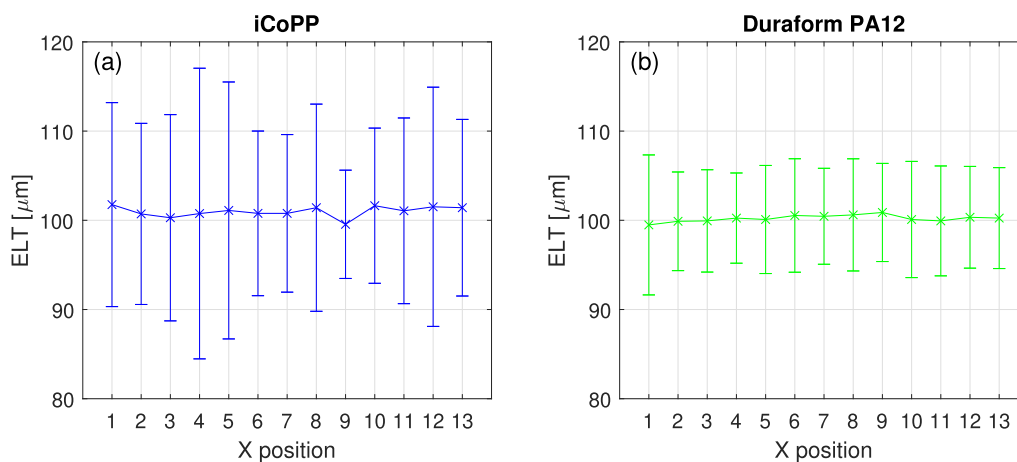


Fig. 17. Evolution of  $ELT$  along  $X$  direction for iCoPP and Duraform PA12. (For interpretation of the references to color in this figure legend, the reader is referred to the web version of this article.)

in Fig. 19. An increase of temperature leads to an increase of powder cohesiveness which, together with the downward pressure of the roller, might explain the increase of  $\rho_p$  for deeper layers observed in both cases.

When considering the respective  $\rho_m$  of the two polymers, the average  $\rho_p$  values for Duraform PA12 and iCoPP are  $0.37 \pm 0.03 \text{ g cm}^{-3}$  and  $0.35 \pm 0.05 \text{ g cm}^{-3}$ . These numbers are higher than previously reported [9]:  $0.26 \pm 0.02 \text{ g cm}^{-3}$  for Duraform PA12 and  $0.29 \pm 0.02 \text{ g cm}^{-3}$

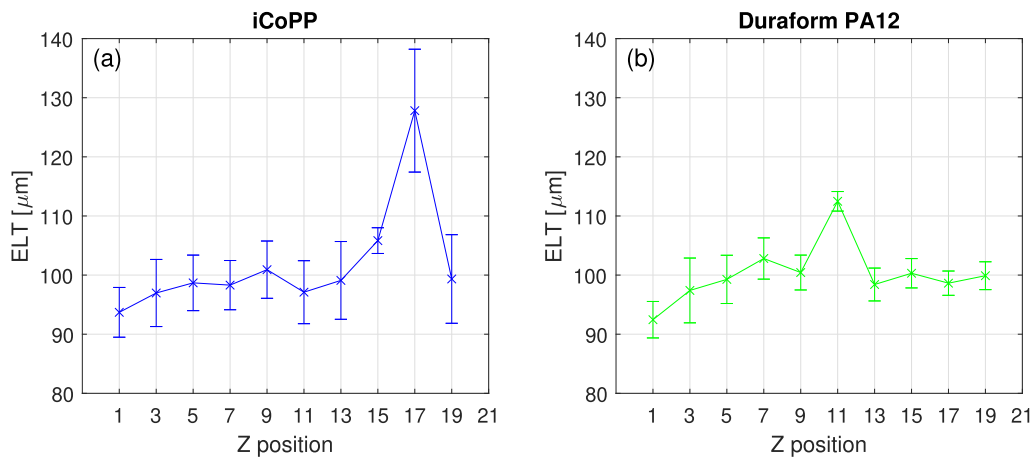


Fig. 18. Evolution of ELT along Z direction for iCoPP (a) and Duraform PA12 (b).

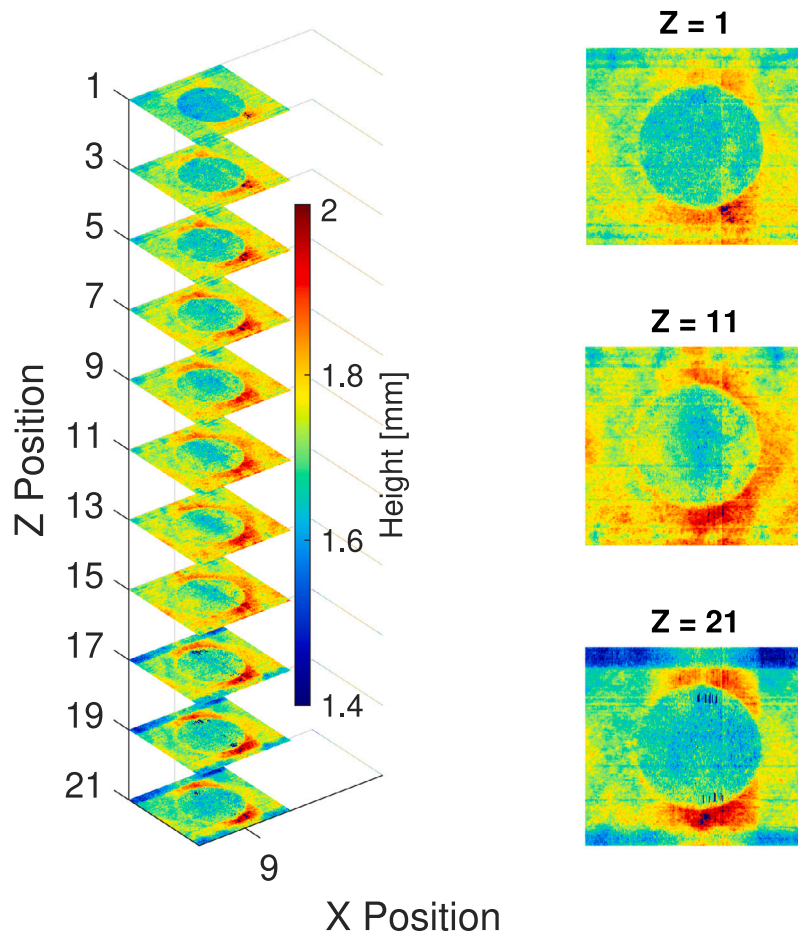


Fig. 19. Example of the vertical evolution of melt pool for Duraform PA12.

for iCoPP. The experimental conditions, and even the measurement procedure, are quite different for these two sets of  $\rho_p$ : in fact, [9] used a blade instead of a roller, and the powder was recoated in a metal cavity with nominal depth approximately equal to 150  $\mu\text{m}$  at room temperature. Given the use of the roller and higher temperatures, the spreading conditions are different in the present work. Another difference comes from the wall effect: as already reported by [27], the cavity does not allow too much rearrangement of the deposited powder, while recoating powder on powder is expected to increase  $\rho_p$  thanks to more rearrangement possibilities. Anyways, albeit these powders have

different Hausner ratios and flowability at room temperature, in the real process conditions they perform quite similarly in terms of  $\rho_p$ , confirming once more how important the reliability of this metric is for the development of new materials for polymer PBF.

Therefore, laser profilometry can be used not only to relatively evaluate  $\rho_p$  by looking at the powder bed  $S_q$ , but the technique also allows for determination of the absolute value with a good level of precision using specific test geometries such as the one proposed in this section.

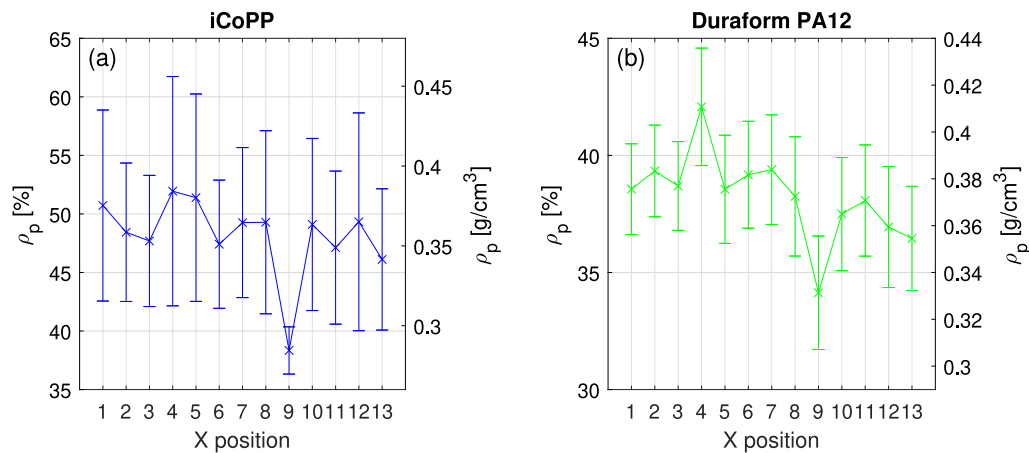


Fig. 20. Evolution of  $\rho_p$  along  $X$  direction for iCoPP and Duraform PA12.

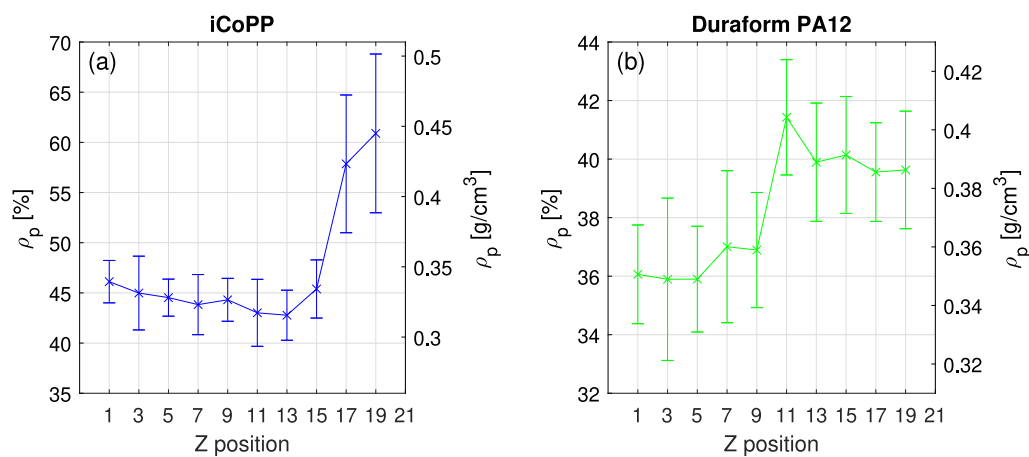


Fig. 21. Evolution of  $\rho_p$  along  $Z$  direction for iCoPP and Duraform PA12.

Table 6

Process parameters for  $\theta$  evaluation.

Parameter	Duraform PA12
Laser power [W]	35
Hatch [mm]	0.24
Laser speed [ $\text{mm s}^{-1}$ ]	4000
Layer thickness [ $\mu\text{m}$ ]	100
Recoating speed [ $\text{mm s}^{-1}$ ]	80
Part bed temperature [ $^{\circ}\text{C}$ ]	173
Feeder temperature [ $^{\circ}\text{C}$ ]	40–60–80 (stable)

### 3.3. Curling monitoring

Three tensile bars according to ISO 527-5 A were produced as outlined in Fig. 6a using the build parameters of Table 6 with Duraform PA12. Despite its large sintering window, even this feedstock can suffer from curling if the wrong process parameters are utilized, and curling is particularly problematic for the development of new materials, which are typically characterized by narrower processing windows [28].

In order to prove the robustness of the proposed curling detection algorithm, the feeder temperature was varied between 40 °C to 80 °C in three different build cycles. An example of the resulting data analysis, carried out according to the procedure introduced above, is shown in Fig. 22.

More details on each height distribution, including their mean and standard deviation, are reported in Table S1.

The complete results in terms of  $\theta$  are shown in Fig. 23 for parts A to C (from left to right of the platform, as depicted in Fig. 6a), with  $T$  being the feeder temperature:

The build cycle had to be stopped after layer 3 for 40 °C and after layer 4 for 60 °C due to excessive curling and consequent collision with the recoater, as shown in Fig. 24a and b, respectively:

There seems to be two main drivers for curling: layer count and temperature. As expected, an increase of temperature decreases  $\theta$ , but if excessive it results in excessive powder cohesiveness and consequently, a deterioration of the powder layer surface roughness. Curling becomes more pronounced with the increase of the layer count, and according to the metric used, values of  $\theta$  above 300  $\mu\text{m}$  are unacceptable and lead to process interruption. Even with the best parameters hereby used, where an experienced operator could not detect any issue, a 75  $\mu\text{m}$  difference could be measured between the reference and the part planes, which probably means that slightly hotter powder would have helped. So, the usage of laser profilometer allows for the rapid and highly resolved determination of the degree of curling. Once interfaced with the machine controls, process monitoring could automatically adapt the temperature of the feeder to minimize  $\theta$  while preserving powder flowability. The maximum  $\theta$  decreases while moving from left to right of the platform (A to C), and in case of part C there seems to be no difference between 40 and 60 °C. This means that placing the parts as far away as possible from the start position of the recoater can help with curling, since the powder gradually heats up during spreading, minimizing the thermal shock for the molten polymer.



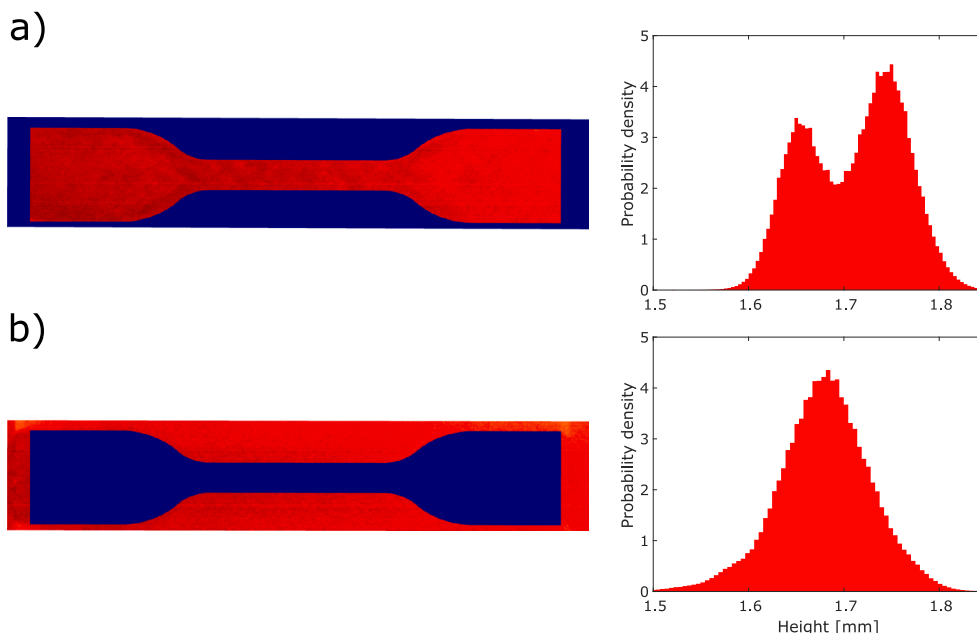


Fig. 22. An example of the raw data after segmentation, showing the inner (a) and outer (b) parts of the tensile bar and their relative height distributions.

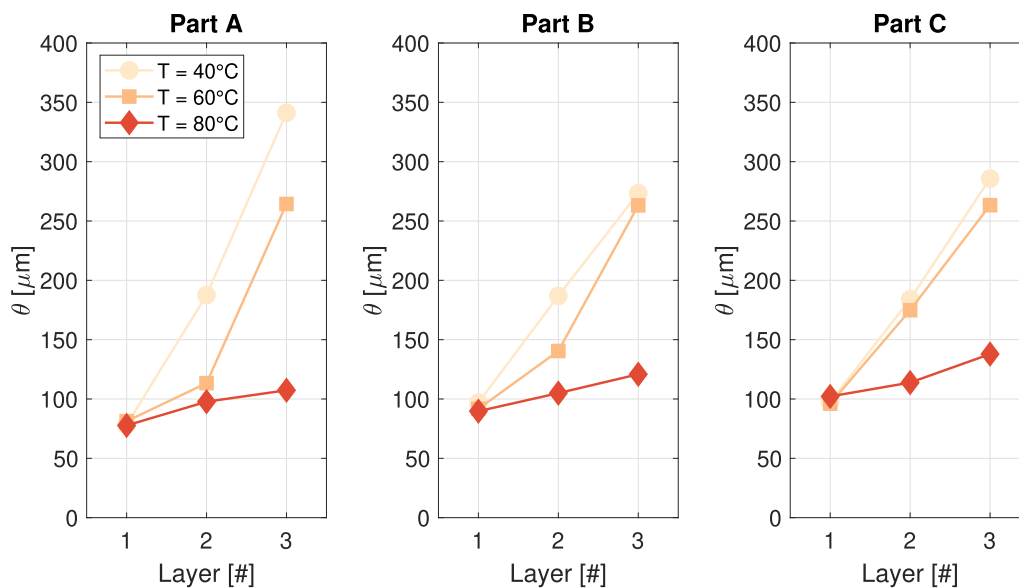


Fig. 23. Curling  $\theta$  as a function of layer count and temperature.

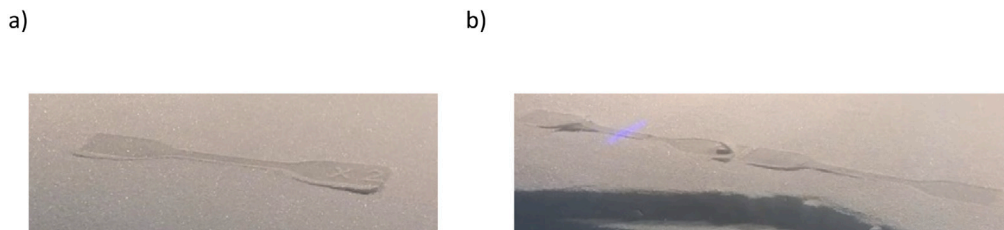


Fig. 24. Curling.

### 3.4. Limitations

Despite being a valid in-situ process monitoring technique, laser profilometry has also some limitations. The most complex one to solve is definitely related to mounting and cooling: this type of devices

needs to be placed relatively close to the powder bed (65 mm in this particular case), and of course cooled down during machine operation. The engineering work required to reliably mount such a device on the recoater is not trivial, and much more complex than installing other process monitoring tools e.g. cameras that can be placed far

away from the processing plane and, possibly, outside of the heated chamber. Also, the maximum acquisition frequency of 16 kHz can be obtained only in specific conditions and, depending on the desired resolution, it can limit the maximum speed if data have to be acquired during the recoating motion. Finally, large files are generated, due to the high *XYZ* resolution of the device: on-the-fly analysis and data reduction techniques must be applied in order to limit the amount of stored data. For example, acquiring a single stripe of 16 mm × 300 mm during a 100 mm tall build cycle with a resolution of 5 μm would take approximately 300 GB, while trying to monitor the entire platform with multiple stripes stitched one next to each other for the same build cycle would result in about 2 TB of raw data.

#### 4. Conclusions and outlook

Process monitoring in additive manufacturing requires tools developed specifically to provide useful data. In this work, laser profilometry was integrated in an industrial LS machine and used to gather data on four metrics: powder layer quality, effective layer thickness, powder layer density, and curling.

Powder layer quality is influenced by temperature and recoating speed depending on the feedstock' particle shape: for Duraform PA12, speed has a detrimental effect on powder layer quality while a higher temperature improves its smoothness. iCoPP, a spherical powder, is not influenced so much by speed in the tested range, but temperature seems to have a detrimental effect. Overall, laser profilometry allows to monitor spreadability in real process conditions, and to tune the recoating parameters (medium, speed) in order to maximize the spreading efficiency while controlling for powder layer quality.

The effective layer thickness *ELT* was measured for the first time during actual PBF of polymers. No variation of *ELT* along the recoating direction was observed, except for the first layer.

The powder layer density  $\rho_p$  was calculated from *ELT* along the recoating and the production directions. Along the former,  $\rho_p$  for Duraform PA12 decreased possibly due to a progressive loss of a fraction of the powder between left and right of the platform, which is expected to worsen for wider platforms and/or less optimized feedstock. Finally, two regimes seemed to exist in the vertical evolution of  $\rho_p$ , with its sharp increase after a certain amount of layers, possibly due to an increase of powder cohesiveness caused by temperature.

Curling  $\theta$  was successfully measured, proving the effectiveness of laser profilometry as multi-purpose process monitoring tool for PBF of polymers. Quantitative information about curling were obtained within the layer time, and used to correct it by acting on the temperature controls. A further reduction is certainly possible by coding the algorithm directly in the control unit of the laser profilometer, which is already built to communicate directly with industrial PLCs. A bi-modal height distribution is found on parts when curling happens, and increasing the preheating temperature has a positive effect on  $\theta$ . Also the placement of the parts as far away as possible from the begin of the recoating motion helps in minimizing  $\theta$ .

In conclusion, laser profilometry features high vertical and lateral resolution, robustness, and easiness of integration into an industrial machine for powder bed fusion, and proved to be a versatile solution for powder and part quality monitoring, both for daily basis operations and for new materials development. The outlook of the present work would be a complete study on dimensional accuracy due to the high lateral resolution of this device, which could be further increased by tuning the process parameters. Improved mechanical integration (i.e. cooling) of the profilometer is required to ensure more complete datasets to understand even more in depth this additive manufacturing process. Finally, machine learning (ML) algorithms will be developed to improve the usage of this technology as process monitoring tool, due to the high amount of high-quality data produced during each layer that is influenced by multiple parameters at the same time.

#### CRediT authorship contribution statement

**Francesco Sillani:** Conceptualisation, Methodology, Software, Validation, Formal analysis, Investigation, Writing – original draft. **Eric MacDonald:** Conceptualisation, Software, Resources, Writing – original draft, Supervision. **Janelly Villela:** Software. **Manfred Schmid:** Writing – review & editing, Supervision. **Konrad Wegener:** Writing – review & editing, Supervision.

#### Declaration of competing interest

The authors declare that they have no known competing financial interests or personal relationships that could have appeared to influence the work reported in this paper.

#### Data availability

Data will be made available on request.

#### Acknowledgments

The authors would like to thank the Murchison Chair at the University of Texas at El Paso and the STARS equipment grant funded by the University of Texas System, USA, and Gaia Alberio for the support in data analysis.

#### Appendix A. Supplementary data

Supplementary material related to this article can be found online at <https://doi.org/10.1016/j.addma.2022.103074>.

#### References

- [1] Erik Westphal, Hermann Seitz, A machine learning method for defect detection and visualization in selective laser sintering based on convolutional neural networks, *Addit. Manuf.* (ISSN: 22148604) 41 (2021) 101965, <http://dx.doi.org/10.1016/j.addma.2021.101965>, URL <https://linkinghub.elsevier.com/retrieve/pii/S2214860421001305>.
- [2] EOS GmbH, EOS formiga P110 velocis, 2022, URL <https://www.eos.info/en/additive-manufacturing/3d-printing-plastic/eos-polymer-systems/formiga-p-110-velocis>.
- [3] EOS GmbH, EOS P500, 2022, URL <https://www.eos.info/en/additive-manufacturing/3d-printing-plastic/eos-polymer-systems/eos-p-500>.
- [4] Daniel Schiochet Nasato, Thorsten Pöschel, Influence of particle shape in additive manufacturing: Discrete element simulations of polyamide 11 and polyamide 12, *Addit. Manuf.* (ISSN: 22148604) 36 (February) (2020) 101421, <http://dx.doi.org/10.1016/j.addma.2020.101421>.
- [5] Alessandro Averardi, Corrado Cola, Steven Eric Zeltmann, Nikhil Gupta, Effect of particle size distribution on the packing of powder beds: A critical discussion relevant to additive manufacturing, *Mater. Today Commun.* (ISSN: 23524928) 24 (2020) <http://dx.doi.org/10.1016/j.mtcomm.2020.100964>.
- [6] Pengfei Tan, Fei Shen, Wei Shian Tey, Kun Zhou, A numerical study on the packing quality of fibre/polymer composite powder for powder bed fusion additive manufacturing, *Virtual Phys. Prototyp.* (ISSN: 17452767) 16 (S1) (2021) S1–S18, <http://dx.doi.org/10.1080/17452759.2021.1922965>.
- [7] T. Niino, Effect of powder compaction in plastic laser sintering fabrication, *Solid Free. Fabr. Symp.* 12 (2009) 193–205, URL <http://edge.rit.edu/content/P10551/public/SFF/SFF2009Proceedings/2009SFFPapers/2009-18-Niino.pdf>.
- [8] Marc Vetterli, Powder Optimization for Laser Sintering: An Insight in Powder Intrinsic and Extrinsic Properties (Ph.D. thesis), ETH Zürich, 2019.
- [9] Francesco Sillani, Ramis Schiegg, Manfred Schmid, Eric MacDonald, Konrad Wegener, Powder surface roughness as proxy for bed density in powder bed fusion of polymers, *Polymers* (ISSN: 2073-4360) 14 (1) (2021) 81, <http://dx.doi.org/10.3390/polym14010081>, URL <https://www.mdpi.com/2073-4360/14/1/81>.
- [10] Michael R. Gardner, Adam Lewis, Jongwan Park, Austin B. McElroy, Arnold D. Estrada, Scott Fish, Joseph J. Beaman, Thomas E. Milner, In situ process monitoring in selective laser sintering using optical coherence tomography, *Opt. Eng.* (ISSN: 0091-3286) 57 (04) (2018) 1, <http://dx.doi.org/10.1117/1.oe.57.4.041407>.
- [11] Tim Marten Wischeropp, Claus Emmelmann, Milan Brandt, Aaron Pateras, Measurement of actual powder layer height and packing density in a single layer in selective laser melting, *Addit. Manuf.* (ISSN: 22148604) 28 (March) (2019) 176–183, <http://dx.doi.org/10.1016/j.addma.2019.04.019>.

- [12] Peter Mercelis, Jean Pierre Kruth, Residual stresses in selective laser sintering and selective laser melting, *Rapid Prototyp. J.* (ISSN: 13552546) 12 (5) (2006) 254–265, <http://dx.doi.org/10.1108/13552540610707013>.
- [13] Shwe P. Soe, Quantitative analysis on SLS part curling using EOS P700 machine, *J. Mater Process. Technol.* (ISSN: 09240136) 212 (11) (2012) 2433–2442, <http://dx.doi.org/10.1016/j.jmatprotec.2012.06.012>,
- [14] Francesco Sillani, Fabian de Gasparo, Manfred Schmid, Konrad Wegener, Influence of packing density and fillers on thermal conductivity of polymer powders for additive manufacturing, *Int. J. Adv. Manuf. Technol.* (ISSN: 14333015) 117 (7–8) (2021) 2049–2058, <http://dx.doi.org/10.1007/s00170-021-07117-z>.
- [15] Sven Helge Klippstein, Florian Heiny, Nagaraju Pashikanti, Monika Gessler, Hans-Joachim Schmid, Powder spread process monitoring in polymer laser sintering and its influences on part properties, *JOM* (ISSN: 1047-4838) (2021) <http://dx.doi.org/10.1007/s11837-021-05042-w>.
- [16] Nicholas Southon, Petros Stavroulakis, Ruth Goodridge, Richard Leach, In-process measurement and monitoring of a polymer laser sintering powder bed with fringe projection, *Mater. Des.* (ISSN: 02641275) 157 (2018) 227–234, <http://dx.doi.org/10.1016/j.matdes.2018.07.053>, URL <https://linkinghub.elsevier.com/retrieve/pii/S0264127518305835>.
- [17] Chris Barrett, Eric MacDonald, Brett Conner, Fred Persi, Micron-level layer-wise surface profilometry to detect porosity defects in powder bed fusion of inconel 718, *JOM* 70 (9) (2018) 1844–1852, <http://dx.doi.org/10.1007/s11837-018-3025-7>.
- [18] Terry Wohlers, Robert Ian Campbell, Olaf Diegel, Joseph Kowen, Ray Huff, Noah Mostow, Wohlers Report 2021, Technical Report, ISBN: 978-0-9913332-7-1, 2021, p. 375, URL <https://wohlersassociates.com/2021report.htm>.
- [19] Manfred Schmid, *Laser Sintering with Plastics*, Hanser Publishers, Munich, ISBN: 978-1-56990-683-5, 2018, p. 194, <http://dx.doi.org/10.3139/9781569906842.fm>.
- [20] H.W. Mindt, M. Megahed, N.P. Lavery, M.A. Holmes, S.G.R. Brown, Powder bed layer characteristics: The overseen first-order process input, *Metall. Mater. Trans. A* (ISSN: 10735623) 47 (8) (2016) 3811–3822, <http://dx.doi.org/10.1007/s11661-016-3470-2>.
- [21] Deniz Jansen, Theresa Hanemann, Markus Radek, Astrid Rota, Jörg Schröpfer, Martin Heilmaier, Development of actual powder layer height depending on nominal layer thicknesses and selection of laser parameters, *J. Mater Process. Technol.* (ISSN: 09240136) 298 (June) (2021) <http://dx.doi.org/10.1016/j.jmatprotec.2021.117305>.
- [22] Fuad Osmanlic, Katrin Wudy, Tobias Laumer, Michael Schmidt, Dietmar Drummer, Carolin Körner, Modeling of laser beam absorption in a polymer powder bed, *Polymers* (ISSN: 20734360) 10 (7) (2018) 1–11, <http://dx.doi.org/10.3390/polym10070784>.
- [23] James E. Mark, *Polymer Data Handbook*, Oxford University Press, Oxford, ISBN: 978-0-19-518101-2, 2009, p. 1264.
- [24] H.J. Yang, P.J. Hwang, S.H. Lee, A study on shrinkage compensation of the SLS process by using the taguchi method, *Int. J. Mach. Tools Manuf.* (ISSN: 08906955) 42 (11) (2002) 1203–1212, [http://dx.doi.org/10.1016/S0890-6955\(02\)00070-6](http://dx.doi.org/10.1016/S0890-6955(02)00070-6).
- [25] M. Schmid, Felipe Amado, Gideon Levy, iCoPP - A new polyolefin for additive manufacturing, SLS, in: *International Conference on Additive Manufacturing*, AM, 2011.
- [26] Dietmar Schulze, *Powders and Bulk Solids*, Springer Berlin Heidelberg New York, ISBN: 978-3-540-73767-4, 2008, p. 517.
- [27] Lukas Haferkamp, Livia Haudenschild, Adriaan Spierings, Konrad Wegener, Kirstin Riener, Stefan Ziegelmeier, Gerhard J. Leichtfried, The influence of particle shape, powder flowability, and powder layer density on part density in laser powder bed fusion, *Metals* (ISSN: 20754701) 11 (3) (2021) 1–15, <http://dx.doi.org/10.3390/met11030418>.
- [28] Rob Kleijnen, Manfred Schmid, Konrad Wegener, Production and processing of a spherical polybutylene terephthalate powder for laser sintering, *Appl. Sci.* (ISSN: 2076-3417) 9 (7) (2019) 1308, <http://dx.doi.org/10.3390/app9071308>, URL <https://www.mdpi.com/2076-3417/9/7/1308>.